physica status solidi a
www.pss-a.com

Check for updates

Photoelectric Generation Coefficient of B-Gallium Oxide during Exposure to High-Energy Ionizing Radiation

Kevin Goodman, Sam McHenry, Jeff Titus, Robert Cooper, Hemant Ghadi, Steve Ringel, Kazuki Nomoto, Wenshen Li, Dobrin P. Bossev, Debdeep Jena, Huili Grace Xing, Matthew J. Gadlage, and Matthew R. Halstead*

For utilization in environments where radiation causes concern, a material's photogeneration coefficient proves essential for device designers. To extract this parameter for gallium oxide, which exhibits higher breakdown voltage characteristics compared with other commonly used semiconductor materials, making it desirable for high-power applications, Schottky diodes receive high-dose-rate radiation from an electron linear accelerator. Monitoring photogenerated charge versus dose rate reveals a photogeneration coefficient of 2.4×10^{15} pairs (cm^{-3}-rad(Si)$^{-1}$) for epitaxially grown β-phase gallium oxide.

1. Introduction

While not new to the scientific community, gallium oxide grasped the attention of many researchers in the past two decades.[1–15] The reason for much of the interest lies in this material's potential for offering solutions to challenges in niche markets. No perfect semiconductor exists for every application. Tradeoffs between cost, reliability, voltage limits, carrier densities and speeds, and photonic behavior, even funding probabilities, all dictate which material a designer or scientist uses for a specific purpose. For gallium oxide, one of the strengths, perhaps the most intriguing this material presents, is its 8 MV cm^{-1} breakdown field.[16] When compared with similar high-voltage-tolerant materials such as gallium nitride and silicon carbide displaying breakdown voltages of 2.5 and 3.3 MV cm^{-1},[16] respectively, one can see why the increased interest.

Within the group of applications in which a high electric field proves necessary, certain environments also demand a second characteristic from materials. Specifically, within environments where high-energy ionizing radiation exists, materials must withstand photocurrent generation to ensure expected performance. Ionizing radiation describes an external electromagnetic (EM) wave or projectile depositing energy into a device as it passes either into or through a material, thus causing the excitation of electrons.[17] The external object may take many forms, neutrons, electrons, protons, energy waves, ions, etc., and occurs in many environments. Space exploration, solar photodetectors,[18–22] nuclear reactor power generation, and strategic events represent popular circumstances where ionizing radiation threatens the proper function of microelectronic devices.[23–28]

As the radiation deposits energy along its path through the material, energy can transfer to native atoms, causing the generation of free electrons. If the excitation occurs within an electric field, either internally such as a p–n junction or external bias, the electrons generated by the radiation form a photogeneration current. This photogeneration current has the capability to manipulate microelectronics, resulting in uncontrolled effects ranging from altering the state of a digital device to inducing photocurrent surges large enough to permanently damage circuitry.[29] In light of this, designers who plan to utilize gallium oxide in such environments must have a means to predict the material's response to high-energy ionizing radiation, thus ensuring that they ordain adequate mitigation strategies.

A parameter of gallium oxide which offers insight into how it behaves in response to high-energy ionizing radiation is its photogeneration coefficient. The photogeneration coefficient of a material correlates how many electrons are freed from their host

K. Goodman, J. Titus
Amentum
13923 E CAPT WJ Nelson Drive, Odon, IN 47562, USA
E-mail: kgoodman@alumni.nd.edu

S. McHenry, R. Cooper, D. P. Bossev, M. J. Gadlage
Naval Surface Warfare Center
300 Highway 361, Crane, IN 47522-5001, USA

H. Ghadi, S. Ringel
Electrical and Computer Engineering Department
The Ohio State University
205 Dreese Labs, 2015 Neil Ave, Columbus, OH 43210, USA

K. Nomoto, W. Li, D. Jena, H. G. Xing
School of Electrical and Computer Engineering
Cornell University
418 Phillips Hall, Ithaca, NY 14853, USA

D. Jena, H. G. Xing
Department of Materials Science Engineering
Cornell University
210 Bard Hall, Ithaca, NY 14853, USA

D. Jena, H. G. Xing
Kavli Institute for Nanoscale Science
Cornell University
245 Feeney Way, Ithaca, NY 14853, USA

M. R. Halstead
Applied Physics Laboratory
Johns Hopkins University
11100 Johns Hopkins Road, Laurel, MD 20723, USA

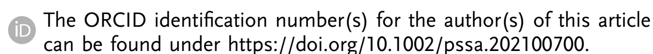
The ORCID identification number(s) for the author(s) of this article can be found under https://doi.org/10.1002/pssa.202100700.

DOI: 10.1002/pssa.202100700

 © 2022 Wiley-VCH GmbH

atoms relative to how much energy is deposited in the material, thus allowing the calculation of potential photocurrent based on the amount of energy deposited by the incident radiation. Herein the controlled irradiations of a gallium oxide Schottky barrier diode (SBD) are described, while monitoring the generated photocurrent. Analysis of these data allowed a means to extract the photogeneration coefficient for the material. A literature search for similar undertakings proved fruitless. This fact combined with the novelty of gallium oxide within the microelectronic community indicates that this may be the first attempt at uncovering the photogeneration coefficient of gallium oxide for high-ionizing-radiation environments.

Equation (1) describes the drift component of the photocurrent generated during a dose of ionizing irradiation while the beam pulse is active.[30] The diffusion current which occurs after the beam pulse, as discussed in the study by Wirth et al., is removed here, as interest only lies in the photocurrent created during the beam pulse for the task at hand. Here, G_{SS} is the product of the dose rate δ and the photogeneration coefficient $\hat{g}$. A and W are the cross-sectional area and depletion region width, respectively, and q represents the electron charge. Integrating Equation (1) over the pulse width, τ, yields the drift-only photogenerated charge, Q_{PP}, created during the pulse. Rearrangement leads to Equation (2), identifying the photogeneration coefficient as the product of known constants and the (photogenerated charge:dose rate) ratio. Shown here, experimentally documenting this ratio allows calculation of the quantity of interest, the photogeneration coefficient of gallium oxide.

$$I_{PP} = q*A*G_{SS}*W \tag{1}$$

$$g = \frac{Q_{PP}}{q*A*W*\delta*\tau} \tag{2}$$

2. Experimental Section

The Ga_2O_3 device wafer originated from Novel Crystal Technology. The structure consisted of 10.4 μm of silicon-doped gallium oxide grown by hydride vapor-phase epitaxy upon a 657 μm-thick substrate of tin-doped (6.8×10^{18} cm^{-3}) gallium oxide. Data indicate that the dopants were activated to yield a carrier concentration of 1.4×10^{16} cm^{-3}. Researchers diced the wafer into cm^2 die. Using these die, SBDs of various types were fabricated by Cornell researchers and the resultant device results are published in previous reports.[31–37] The planar SBDs typically exhibited a breakdown voltage near 600 V, defined at a leakage current level of 1 mA cm^{-2}, while the trench SBDs had a breakdown voltage up to 3000 V. Ti/Au (50/100 nm) metals constituted an ohmic contact to the substrate, while Ni/Au (40/150 nm) metals enabled a Schottky junction to the epitaxial layer. Liftoff procedures patterned the Schottky metals into circular contacts of varying diameters, 30, 80, 180, and 360 μm, as displayed in Figure 2. Of importance here were contacts with 180 μm diameter. The ohmic contact remained planar on the backside of the sample. **Figure 1** demonstrates rectifying behavior from the diode prior to irradiation, while detailed electrical characterization of the material remained in a prior letter.[31]

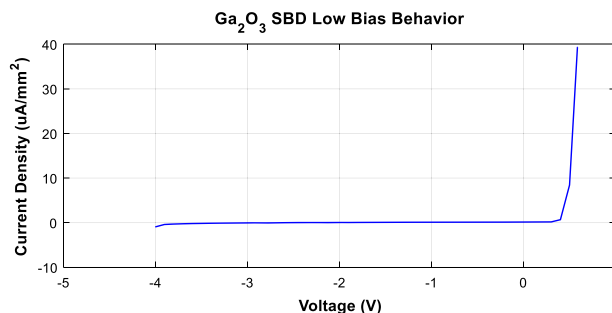

Figure 1. Low-bias behavior of gallium oxide Schottky diode.

For this experiment, silver paste conductively attached the ohmic contact to a dual inline package (DIP). Gold wire bonds connected five of the 180 μm Schottky contacts to the DIP leads. These five leads terminated together, forming an effective surface area of 0.127 mm^2 for the Schottky contact to the epitaxial layer. A gold wire bond also connected the Ohmic contact to DIP socket leads, as visible in the upper-right corner of **Figure 2**, which displays an enhanced image of the patterned sample wire bonded to the DIP leads.

Irradiation occurred via a 23 MeV L-band electron linear accelerator (Linac) operating at 1.3 GHz. The variation of dose rate occurred by changing the distance between the Linac aperture and the device under test (DUT) as beam intensity decreased as distance^{-2} with respect to distance from the irradiation source.[38] Prior to DUT irradiation, calcium fluoride (CaF_2) dosimeters received irradiation in place of the DUT at various

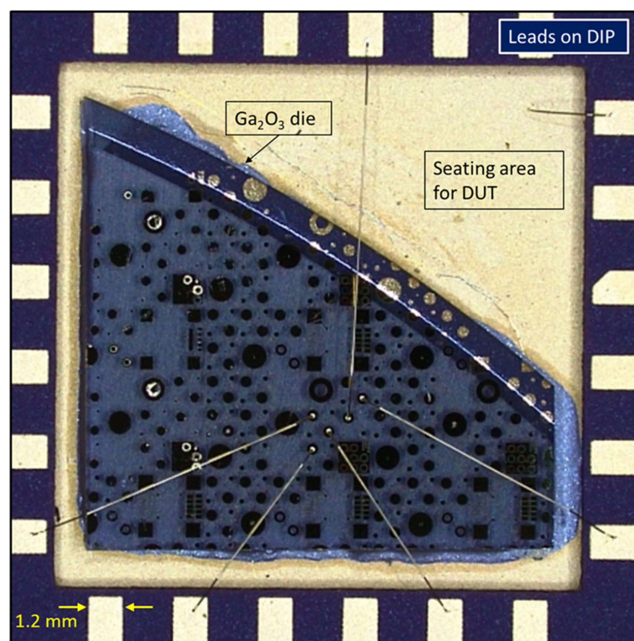

Figure 2. Optical top-view image of the gallium oxide die bonded to the DIP. The patterned Schottky metal contacts reside on the top surface, facing the irradiation source, while the blanket Ohmic contact resides on the backside of the gallium oxide die in direct contact with the seating area of the DIP.

 © 2022 Wiley-VCH GmbH

distances from the beam aperture. Standardizing the photoemission of these CaF_2 dosimeters against others excited by irradiation sources of known dose rates[39] allowed calibration of a p–i–n diode sitting behind the DUT to quantify approximate dose rates at different distances from the beam aperture.

Exposures occurred under specific reverse bias conditions for each dose rate. Electrical contact occurred as follows. Being wire bonded into the DIP, the diode resided in a printed circuit board (PCB) mount, enabling signal interface. To extract the amount of photocurrent generated within the diode, a 10 kΩ sense resistor resided along the diode's current path, supplying a voltage signal to an oscilloscope. **Figure 3** displays a schematic of the test circuit that contained the board and DIP. A Keithley 2410 power supply provided potential to the circuit. Due to the harsh environment and to limit its exposure, the power supply sat ≈50 ft. away from the beam in a shielded control room and was connected to the test circuit via shielded cables. To minimize the effects of this cable, four 0.1 and six 0.01 μF ceramic capacitors resided adjacent to the Schottky diode test package. The use of capacitors provided immediate charge during the Linac pulse and maintained the test circuit bias during the pulse. A lead plate with an orifice centered over the diode protected the PCB electronics, limiting their exposure to irradiation. The signal from the sense resistor traveled 50 feet along the coax cable to the control room. A Tektronix DPO7104C oscilloscope terminated at 1 MΩ captured the signal.

Upon capture, the data ran through 100-point averaging filter to remove high-frequency noise from the recorded signal, which stemmed from the beam formation in the Linac. **Figure 4** demonstrates the result of the filter once applied to a representative data capture.

3. Results and Discussion

If one ascertains the semiconductor doping, N_d, and the diode's built in potential, V_{bi}, this information combines with Equation (3) to determine how the applied bias dictates the width of the depletion region, W.[40] Upon knowing the depletion region width, the photogeneration coefficient of gallium oxide, a constant material parameter, becomes attainable using Equation (2). The dielectric coefficient value used in the calculation, 10.0, originated from other studies.[41,42]

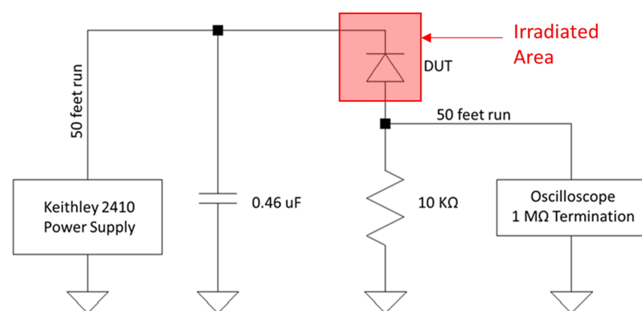

Figure 3. Schematic of the test circuit.

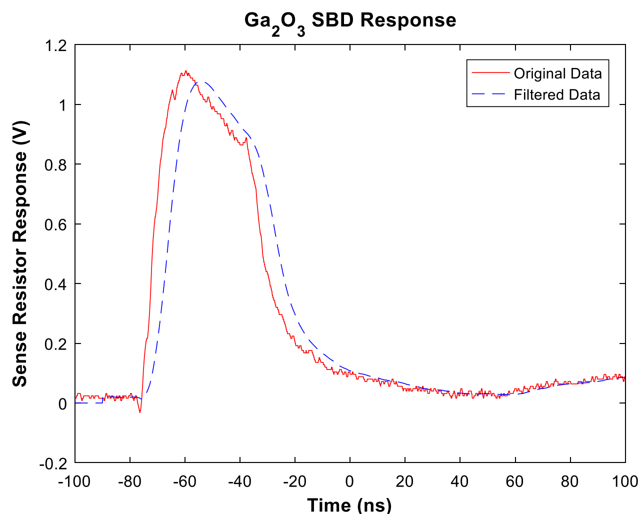

Figure 4. Example of device response demonstrating filtering of the signal.

$$W = \sqrt{[2 * \varepsilon * \frac{Vbi - Vapp}{q * Nd}]} \quad (3)$$

Capacitance versus voltage measurements in **Figure 5** reveal these two values of importance. As marked in **Figure 6**, plotting $1/C^2$ normalized to contact area versus reverse bias yields the built-in voltage from the plot's x-intercept. Utilizing Equation (4) offers carrier concentration from the slope of this line.[40] Here q and ε represent the same constants as earlier. Upon plotting the capacitance-voltage (CV) data, the doping and built-in voltage values cypher to 1.4×10^{16} cm^{-3} and 1.43 V, respectively.

$$N_d = \left(\frac{2}{q * \varepsilon s}\right) * \left(-\frac{1}{\frac{d(\frac{1}{C^2})}{dV}}\right) \quad (4)$$

Extracting the quantitative value of photocurrent generated per dose from data curves, as depicted in Figure 4, occurred by first removing the quiescent voltage. Dividing this left over dynamic signal by the value of the sense resistor, 10 kOhm, yields photocurrent plotted versus time. A Matlab program integrated the I_{PP} versus time plot over the definite time integral starting at $Time_{Beam\text{-}On}$ and ending at $Time_{Beam\text{-}Off}$. As the diffusion current

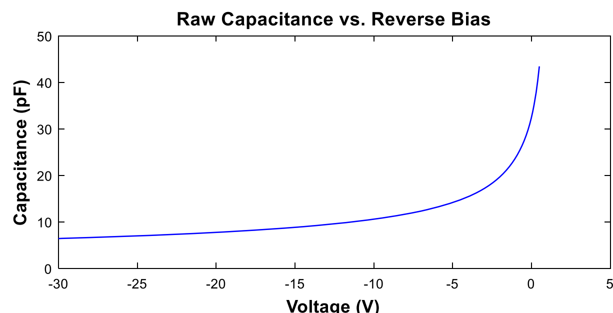

Figure 5. Raw capacitance data plotted against reverse bias.

© 2022 Wiley-VCH GmbH

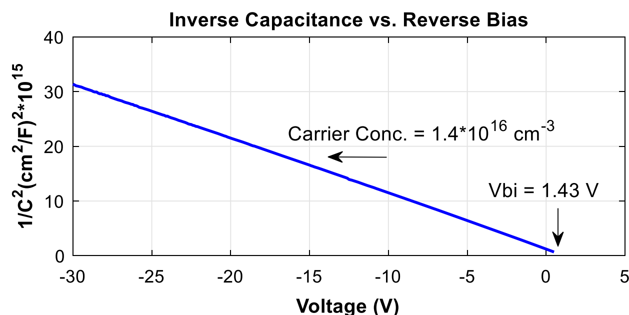

Figure 6. Inverse of capacitance squared normalized to surface area plotted against reverse bias of the diode.

portion of the photocurrent occurs after the irradiation pulse,[30] integrating over only the pulse width offers the desired result, the drift-only portion of the photocharge generated by each irradiation. **Figure 7** displays these photocharge values generated during each irradiation versus the dose rate received during irradiation parceled by each bias condition. Each point represents a single irradiation dose and the slopes show linear regressions of these data. Each slope shown represents data from a specific reverse bias on the diode; therefore, each slope represents data from a unique depletion region width. As there is no photocurrent at zero dosage, the linear regression for the slopes has been forced through zero.

Figure 8 combines the slopes of the photocharge versus dose rate taken from Figure 7 at each bias into the same plot offering a sanity check on the data. This demonstrates that as the reverse bias is increased, the photocurrent also increases as it should, as the depletion region in the gallium oxide increases.

The slopes from Figure 7 offer the $\{Q_{PP}$:dose rate$\}$ ratio needed for use in Equation (2) to yield the photogeneration coefficient. As all other values were known, using this ratio in Equation (2) yields direct values for the photogeneration coefficient. Plotting this value for each reverse bias leads to **Figure 9**, where the error bars represent 95% confidence intervals. Note that as the reverse bias reaches 21 V, the photogeneration coefficient appears to increase. An untested hypothesis is that the increase might be due to increasingly exacerbated field crowding with increasing reverse bias, as observed by others in the industry where Ga_2O_3 diodes see edge effects at the anode edges, thus shaping the electric field lines in nonuniform ways.[35–37] This observation combined with the large standard deviation seen at higher voltages recommends removing these data from the

Figure 7. Photocharge versus dose rate separated by biasing conditions. Each data point represents one dose of irradiation. The slopes of the plots are indicated in each legend. Absolute values not shown due to export-control requirements.

© 2022 Wiley-VCH GmbH

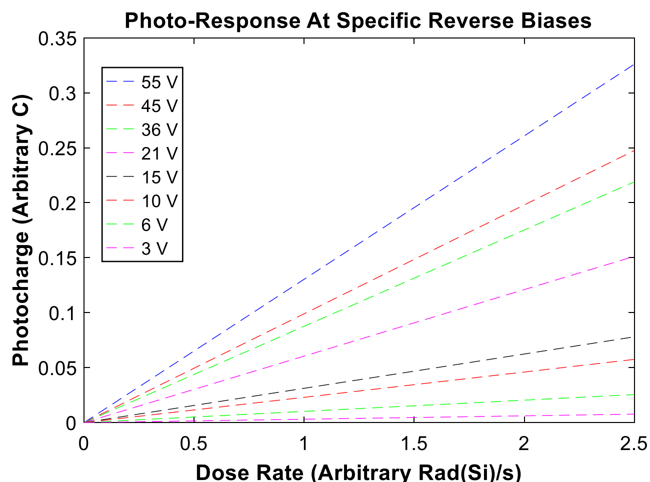

Figure 8. Photogenerated charge versus dose rate at various voltages. Note that reverse bias increases as does the generated photocurrent as it physically should due to a larger depletion width and therefore more collection volume.

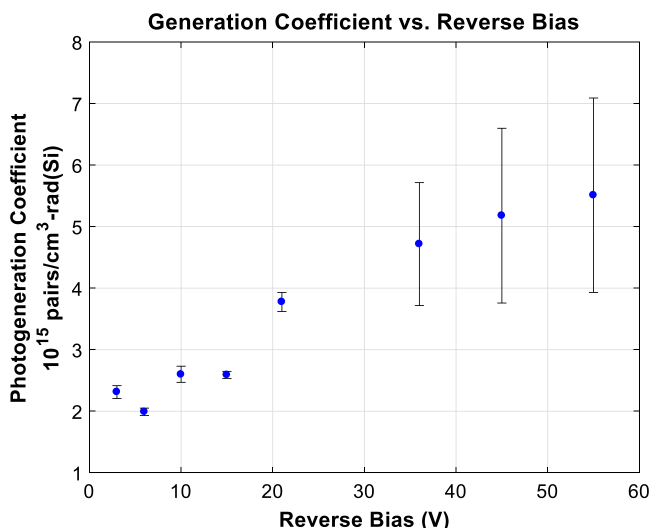

Figure 9. Photogeneration coefficient averaged at each reverse bias with 95% confidence intervals. Notice the steady increase of the value above 21 V.

final calculation. Note that the large standard deviation at high biases is due in part to a small sampling of data.

Moving forward, utilizing biasing conditions below 20 Volts offers, as shown in **Figure 10**, leading to an average value of 2.4×10^{15}, electron–hole pairs per cubic centimeter-rad(Si) for the photogeneration coefficient of ß-gallium oxide exposed to high-energy electrons. As discussed, upon higher diode reverse biasing, experimental data show the value of the photogeneration coefficient increase with bias. Therefore, the 2.4×10^{15} value should be viewed as the low appraise when one designs Ga_2O_3 radiation-tolerant devices. Offering a reference value for comparison,[43] silicon hosts a photogeneration coefficient of 4.0×10^{13} pair per cubic centimeter-rad(Si). Therefore,

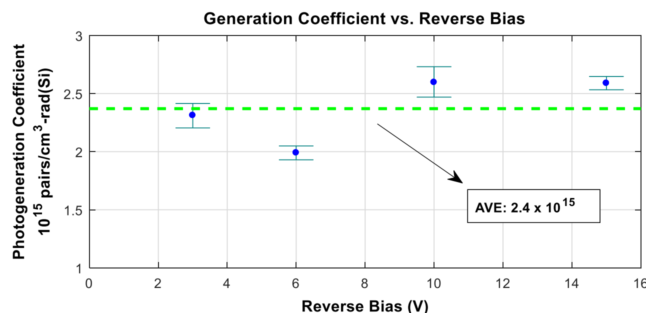

Figure 10. Photogeneration coefficient averaged at each reverse bias along with 95% confidence intervals. The dashed blue line represents the overall average value.

authors caution designers that the photogeneration coefficient value utilized for silicon (historically the most common material utilized in radiation environments) proves inappropriate for gallium oxide applications.

4. Conclusion

Hydride vapor-phase epitaxy β-gallium oxide SBDs generated photoinduced charges when irradiated with high-energy linear accelerated electrons. This radiation setup duplicates device operation in high-energy-ionizing surroundings such as high-power electromagnetic pulse environments. Plotting the photocharge versus dose rate while holding the diode under multiple reverse-bias voltages revealed a photogeneration coefficient of 2.4×10^{15} pairs (cm^{-3}-rad(Si)$^{-1}$) for β-gallium oxide when exposed to high-energy ionizing radiation environments. Experiments saw this value increase at higher reverse biases, possibly due to field crowding near the anode edges of the diode. Identification of this value assists designers to predict gallium oxide device behavior in high-energy ionizing environments and thus tailor devices to perform with anticipated behavior in such environments. It is noteworthy that the comparison of this photogeneration coefficient with values of other popular wide-bandgap semiconductors proved difficult due to lacking the availability of substantial literature on the subject. With this in mind, the authors herein encourage the radiation community to investigate dose rate consequences generated by high-energy ionizing radiation within wide-bandgap and other novel microelectronic materials.

Acknowledgements

Irradiation and data collection/analysis occurred at Crane NSWC and were supported by Naval Innovative Science & Engineering Program award 19-CR-WD-0056. CV data measurements occurred at Ohio State University. Device fabrication work at Cornell was supported by the AFOSR/Cornell Center of Excellence (grant no. FA9550-18-1-0529, Program Officer: Dr. Ali Sayir) and AFOSR grant no. FA9550-20-1-0148 (Program Officer: Dr. Kenneth Goretta), using CNF and CCMR Shared Facilities sponsored by the NSF NNCI program (no. ECCS-1542081), MRSEC program (no. DMR-1719875), and MRI (no. DMR-1338010).

© 2022 Wiley-VCH GmbH

Conflict of Interest

The authors declare no conflict of interest.

Data Availability Statement

The data that support the findings of this study are available from the corresponding author upon reasonable request.

Keywords

gallium oxide, ionizing radiation, photogeneration coefficients

Received: October 14, 2021
Revised: January 10, 2022
Published online: February 9, 2022

[1] H. S. Oon, K. Y. Cheong, *Mater. Sci. Semicond. Process.* **2013**, *16*, 1217.
[2] S. Garud, N. Gampa, T. G. Allen, R. Kotipalli, D. Flandre, M. Batuk, J. Hadermann, M. Meuris, J. Poortmans, A. Smets, B. Vermang, *Phys. Status Solidi A* **2018**, *215*, 1700826.
[3] W. Seiler, M. Selmane, K. Abdelouhadi, J. Perrière, *Thin Solid Films* **2015**, *589*, 556.
[4] S. P. Chang, K. J. Chen, *Nanosci. Nanotechnol. Lett.* **2014**, *6*, 914.
[5] Q. Guo, K. Nishihagi, Z. Chen, K. Saito, T. Tanaka, *Thin Solid Films* **2017**, *639*, 123.
[6] S. D. Ponja, S. Sathasivam, I. P. Parkin, C. J. Carmalt, *Sci. Rep.* **2020**, *10*, 1.
[7] L. Sun, M. Zhao, F. Wang, W. Jiang, J. Guo, J. Li, J. Dai, *J. Nanosci. Nanotechnol.* **2020**, *20*, 2395.
[8] J. Wang, W. Li, H. Zhang, Y. Xiong, L. Ye, H. Ruan, G. Qin, C. Kong, *Appl. Phys. A* **2020**, *126*, 1.
[9] Z. Guo, A. Verma, X. Wu, F. Sun, A. Hickman, T. Masui, A. Kuramata, M. Higashiwaki, D. Jena, T. Luo, *Appl. Phys. Lett.* **2015**, *106*, 111909.
[10] V. Balakrishnan, *Doctoral Dissertation*, Cornell University, **2019**.
[11] H. Hu, C. Wu, N. Zhao, Z. Zhu, P. Li, S. Wang, W. Tang, D. Guo, *Phys. Status Solidi A* **2021**, *218*, 2100076.
[12] C. Wu, L. Qiu, S. Li, D. Guo, P. Li, S. Wang, P. Du, Z. Chen, A. Liu, X. Wang, H. Wu, *Mater. Today Phys.* **2021**, *17*, 100335.
[13] K. Zhang, Z. Xu, J. Zhao, H. Wang, J. Hao, S. Zhang, H. Cheng, B. Dong, *J. Alloys Compd.* **2021**, 160665.
[14] X. Y. Zhang, T. He, J. Zhao, G. Liu, Z. L. Wang, C. Zhang, *Mater. Today Phys.* **2020**, *16*, 100295.
[15] C. Wu, D. Y. Guo, L. Y. Zhang, P. G. Li, F. B. Zhang, C. K. Tan, S. L. Wang, A. P. Liu, F. M. Wu, W. H. Tang, *Appl. Phys. Lett.* **2020**, *116*, 072102.
[16] M. Higashiwaki, K. Sasaki, A. Kuramata, T. Masui, S. Yamakoshi, *Appl. Phys. Lett.* **2012**, *100*, 013504.
[17] R. K. Freitag, D. B. Brown, *IEEE Trans. Nucl. Sci.* **1998**, *45*, 2649.
[18] D. A. Bauman, A. I. Borodkin, A. A. Petrenko, D. I. Panov, A. V. Kremleva, V. A. Spiridonov, D. A. Zakgeim, M. V. Silnikov, M. A. Odnoblyudov, A. E. Romanov, V. E. Bougrov, *Acta Astronaut.* **2021**, *180*, 125.
[19] G. Korotcenkov, *Gallium Oxide: Technology, Devices and Applications*, Elsevier, Amsterdam **2018**.
[20] Y. Qin, L. Li, X. Zhao, G. S. Tompa, H. Dong, G. Jian, Q. He, P. Tan, X. Hou, Z. Zhang, S. Yu, *ACS Photonics* **2020**, *7*, 812.
[21] Y. Qin, H. Sun, S. Long, G. S. Tompa, T. Salagaj, H. Dong, Q. He, G. Jian, Q. Liu, H. Lv, M. Liu, *IEEE Electron Device Lett.* **2019**, *40*, 1475.
[22] J. Xu, W. Zheng, F. Huang, *J. Mater. Chem. C* **2019**, *7*, 8753.
[23] J. R. Srour, J. M. McGarrity, *Proc. IEEE*, **1988**, *76*, 1443.
[24] A. H. Johnston, *IEEE Trans. Nucl. Sci.* **1998**, *45*, 1339.
[25] R. D. Schrimpf, *Radiation Effects on Embedded Systems*, Springer, Dordrecht **2007**, pp. 11–29.
[26] P. S. Winokur, G. K. Lum, M. R. Shaneyfelt, F. W. Sexton, G. L. Hash, L. Scott, *IEEE Trans. Nucl. Sci.* **1999**, *46*, 1494.
[27] D. M. Fleetwood, P. S. Winokur, P. E. Dodd, *Microelectron. Reliab.* **2000**, *40*, 17.
[28] P. V. Dressendorfer, *Nucl. Instrum. Methods Phys. Res., Sect. B* **1989**, *40*, 1291.
[29] C. R. Jenkins, D. L. Durgin, *IEEE Trans. Nucl. Sci.* **1977**, *24*, 2361.
[30] J. L. Wirth, S. C. Rogers, *IEEE Trans. Nucl. Sci.* **1964**, *11*, 24.
[31] W. Li, Z. Hu, K. Nomoto, Z. Zhang, J. Y. Hsu, Q. T. Thieu, K. Sasaki, A. Kuramata, D. Jena, H. G. Xing, *Appl. Phys. Lett.* **2018**, *113*, 202101.
[32] W. Li, K. Nomoto, Z. Hu, D. Jena, H. G. Xing, *Appl. Phys. Express* **2019**, *12*, 061007.
[33] W. Li, Z. Hu, K. Nomoto, R. Jinno, Z. Zhang, T. Q. Tu, K. Sasaki, A. Kuramata, D. Jena, H. G. Xing, in *2018 IEEE Inter. Electron Devices Meeting (IEDM)*, IEEE, San Francisco December 2018, pp. 8–5.
[34] W. Li, K. Nomoto, Z. Hu, D. Jena, H. G. Xing, *IEEE Electron Device Lett.* **2019**, *41*, 107.
[35] W. Li, K. Nomoto, Z. Hu, D. Jena, H. G. Barrier Xing, in *IEEE Device Research Conf. (DRC)*, Ann Arbor **2019**, https://doi.org/10.1109/DRC46940.2019.9046433.
[36] W. Li, K. Nomoto, D. Jena, H. G. Xing, *Appl. Phys. Lett.* **2020**, *117*, 222104.
[37] W. Li, K. Nomoto, Z. Hu, D. Jena, H. G. Xing, *IEEE Trans. Electron Devices* **2020**, *67*, 3938.
[38] N. Voudoukis, S. Oikonomidis, *Eur. J. Eng. Technol. Res.* **2017**, *2*, 23.
[39] H. Tugay, Z. E. H. Yegingil, R. A., T. A. M. E. R. Dogan, N. Nur, N. Yazici, *Nucl. Instrum. Methods Phys. Res., Sect. B* **2009**, *267*, 3640.
[40] S. M. Sze, *Semiconductor Devices, Physics and Technology*, John Wiley & Sons Inc. New York, NY **1985**.
[41] M. Passlack, E. F. Schubert, W. S. Hobson, M. Hong, N. Moriya, S. N. G. Chu, K. Konstadinidis, J. P. Mannaerts, M. L. Schnoes, G. J. Zydzik, *J. Appl. Phys.* **1995**, *77*, 686.
[42] A. Fiedler, R. Schewski, Z. Galazka, K. Irmscher, *ECS J. Solid State Sci. Technol.* **2019**, *8*, Q3083.
[43] G. C. Messenger, M. S. Ash, *The Effects of Radiation on Electronic Systems*, Springer, New York, NY **2006**.

 © 2022 Wiley-VCH GmbH